

# Quantum Computational Phase Transition in Combinatorial Problems

Bingzhi Zhang<sup>1,2</sup>, Akira Sone<sup>3</sup>, and Quntao Zhuang<sup>1,4\*</sup>

<sup>1</sup>*Department of Electrical and Computer Engineering,  
University of Arizona, Tucson, Arizona 85721, USA*

<sup>2</sup>*Department of Physics, University of Arizona, Tucson, AZ 85721, USA*

<sup>3</sup>*Aliro Technologies, Inc, Boston, MA 02135, USA and*

<sup>4</sup>*James C. Wyant College of Optical Sciences, University of Arizona, Tucson, AZ 85721, USA*

Quantum Approximate Optimization algorithm (QAOA) is one of the candidates to achieve a near-term quantum advantage. To search for such a quantum advantage in solving any problem, it is crucial to first understand the difference between problem instances' empirical hardness for QAOA and classical algorithms. We identify a computational phase transition of QAOA when solving hard problems such as 3-SAT—the performance is worst at the well-known SAT-UNSAT phase transition, where the hardest instances lie. We connect the transition to the controllability and the complexity of QAOA circuits. Such a transition is absent for 2-SAT and QAOA achieves close to perfect performance at the problem size we studied. Then, we show that the high problem density region, which limits QAOA's performance in hard optimization problems (*reachability deficits*), is actually a good place to utilize QAOA: its approximation ratio has a much slower decay with the problem density, compared to classical approximate algorithms. Indeed, it is exactly in this region that quantum advantages of QAOA can be identified. The computational phase transition generalizes to other Hamiltonian-based algorithms, such as the quantum adiabatic algorithm.

## I. INTRODUCTION

Quantum Approximate Optimization algorithm (QAOA) [1], like all quantum algorithms, aims to utilize quantum hardware to efficiently solve problems that are hard on classical computers. It is one of the candidates to achieve a quantum supremacy in the noisy intermediate-scale quantum (NISQ) era [2]. So far, quantum supremacy has only been realized for random circuit sampling tasks [3, 4]. For complex but practical problems in the class of nondeterministic-polynomial (NP) time, no quantum advantage has been found, despite trials of QAOA on the Google Sycamore quantum processor [5]. To search for quantum supremacy, it is crucial to first understand the difference between what is hard or easy for QAOA and for classical algorithms, which can be best explored via the combinatorial problem of Boolean satisfiability problem (SAT).

In a  $k$ -SAT instance, one asks whether multiple clauses, each involving  $k$  Boolean variables, can be satisfied simultaneously. Depending on the value of  $k$ , the worst-case hardness is drastically different—while 3-SAT is NP-complete, 2-SAT can be efficiently solved in polynomial time (class P). In addition, the classical empirical hardness of random 3-SAT instances is known to have a computational phase transition [6–10] versus the problem density characterized by the clause-to-variable ratio. When the density is small (large), almost all instances are satisfied (unsatisfied) and easy to solve; while for density approaching the critical point of the SAT-UNSAT phase transition, the 3-SAT problem instances become the hardest to solve.

For quantum algorithms such as QAOA, the above phenomenon is largely unexplored. To begin with, as QAOA always implements SAT problems in their NP-hard optimization versions (Max-SAT) [11], it is unclear whether the decision version's NP ( $k = 3$ ) versus P ( $k = 2$ ) contrast has any influence on QAOA's performance. It is also unclear how classical empirical hardness of 3-SAT connects to QAOA's performance on its optimization versions. Indeed, Ref. [12] does not find a big difference between QAOA's performance on Max-2-SAT and Max-3-SAT, and only finds QAOA's performance to worsen as the density increases—a phenomenon they call *reachability deficits*.

In this paper, we reveal a computational phase transition in both the trainability and accuracy of QAOA in solving the positive 1-in- $k$  SAT problem. In terms of trainability characterized by gradient, the typical amplitude of gradient in training 3-SAT achieves the minimum at the critical problem density ratio of the SAT-UNSAT phase transition [6–10], where the instances are hardest classically. However, the gradient in training 2-SAT achieves the minimum amplitude well above the critical point of the SAT-UNSAT transition. We link this gradient transition to the controllability of the quantum systems evolving under the QAOA circuit [13–16] and the complexity of QAOA circuit [17–20]. In terms of accuracy of the optimization versions of SAT, we find the QAOA's approximation ratio to be robust and decay slowly with the problem density. Moreover, despite the performance decay due to reachability deficits, it is precisely in the large problem density region where a quantum advantage can be identified. In addition, the accuracy in solving Max-2-SAT is higher than that in solving Max-3-SAT, consistent with the P versus NP contrast in the decision version of the problems.

The computational phase transition in QAOA's per-

\* zhuangquntao@email.arizona.edu

formance is a quantum generalization of the computational phase transition in classical algorithms [6–10] and reveals the intrinsic hardness of the problem. We expect other Hamiltonian-based quantum algorithms to possess the same phenomenon, as we also confirmed in the case of quantum adiabatic algorithms (QAA) [21–23].

## II. PRELIMINARY

### A. Quantum Approximate Optimization algorithm

To solve an optimization problem, QAOA encodes the cost function into the energy of a problem Hamiltonian  $H_C$ , defined over spin-1/2 particles (qubits), and then seeks for an approximation of the ground state that encodes the solution to the optimization problem. An  $n$ -qubit QAOA circuit implements dynamics governed by the problem Hamiltonian  $H_C$  and a mixing Hamiltonian  $H_B = \sum_{i=1}^n \sigma_i^x$  alternatively in each layer, where  $\sigma_i^x$  is the Pauli- $X$  operator representing the transverse fields. The output state of a  $p$ -layer QAOA is therefore  $|\psi(\vec{\gamma}, \vec{\beta})\rangle = \prod_{\ell=1}^p e^{-i\beta_\ell H_B} e^{-i\gamma_\ell H_C} |\psi(0, 0)\rangle$ , where  $\vec{\gamma} = (\gamma_1, \dots, \gamma_p)$  and  $\vec{\beta} = (\beta_1, \dots, \beta_p)$  are variational parameters. The initial state is set to be a superposition of all possible spin configurations,  $|\psi(0, 0)\rangle = |+\rangle^{\otimes n}$  with  $|+\rangle = (|0\rangle + |1\rangle)/\sqrt{2}$ . To solve the problem, variational training is performed over the parameters  $\vec{\gamma}, \vec{\beta}$  to minimize the cost function  $\mathcal{C}(\vec{\gamma}, \vec{\beta}) = \langle \psi(\vec{\gamma}, \vec{\beta}) | H_C | \psi(\vec{\gamma}, \vec{\beta}) \rangle$ . The variational training terminates when the cost function stops to decrease significantly, and ideally leads to the optimal parameters  $\vec{\gamma}^*, \vec{\beta}^* = \text{argmin}_{\vec{\gamma}, \vec{\beta}} \mathcal{C}(\vec{\gamma}, \vec{\beta})$ .

### B. Positive 1-in- $k$ SAT

We are interested in the positive 1-in- $k$  SAT problem (1- $k$ -SAT<sup>+</sup>,  $k \geq 2$ ), also known as the exact-cover  $k$  problem. Given  $n$  Boolean variables  $V = \{v_i\}_{i=1}^n$ , a random instance of 1- $k$ -SAT<sup>+</sup> can be constructed by choosing  $m$  clauses  $C = \{c_a\}_{a=1}^m$ , each containing  $k$  different variables  $\{v_{aj}\}_{j=1}^k$  in positive literals uniformly randomly chosen from  $V$ . The conjunctive normal form (CNF) of the 1- $k$ -SAT<sup>+</sup> instance can be expressed as  $F(V) = \bigwedge_{a=1}^m c_a(\{v_{aj}\}_{j=1}^k)$ , where ‘ $\bigwedge$ ’ denotes AND and forces the CNF to be true only when all clauses are satisfied. A clause  $c_a(\{v_{aj}\}_{j=1}^k)$  is satisfied if and only if a single variable among  $\{v_{aj}\}_{j=1}^k$  is taken to be true. The (decision version of) 1- $k$ -SAT<sup>+</sup> problem asks whether  $F(V)$  can be satisfied with an assignment of variables  $V$ , while the optimization version—Max-1- $k$ -SAT<sup>+</sup>—aims to find an assignment of variables  $V$  to minimize the number of clause violations. With the increase of clause-to-variable ratio  $m/n$ , it becomes harder to satisfy a random 1- $k$ -SAT<sup>+</sup> instance, and there exists a phase transition of SAT probability across a critical ratio,  $m/n \sim 0.55$  for  $k = 2$  and  $m/n \sim 0.62$  for  $k = 3$  [10],

as shown in Fig. 1(a)(b).

We study the case of  $k = 2$  and  $k = 3$  for a comparison: while 1-2-SAT<sup>+</sup> is in class P and efficiently solvable, 1-3-SAT<sup>+</sup> is NP-complete and it takes an exponential amount of time to solve it, e.g., by the well-known algorithm X [24]. Despite the contrast in the decision versions, Max-1- $k$ -SAT<sup>+</sup> is always NP hard, even for  $k = 2$  [25]. In addition to the worst case hardness, empirical studies with classical algorithms on different variants of 3-SAT [6–10] show that when  $m/n$  is small (large), almost all instances are satisfied (unsatisfied) and easy to solve; while for  $m/n$  approaching the critical point of the SAT-UNSAT transition, the SAT problem instances become the hardest to solve.

To solve SAT problems with QAOA, we transform each Boolean variable  $v_i$  to the spin states of a qubit, with spin-down state  $|1\rangle$  (Pauli-Z operator  $\sigma^z = -1$ ) for true and spin-up state  $|0\rangle$  ( $\sigma^z = 1$ ) for false, and obtain the Ising Hamiltonians for 1-3-SAT<sup>+</sup> and 1-2-SAT<sup>+</sup> as [21–23, 26] (see Appendix A)

$$H_{C,3} = \frac{1}{4} \sum_{a=1}^m (\sigma_{a1}^z + \sigma_{a2}^z + \sigma_{a3}^z - 1)^2, \quad (1a)$$

$$H_{C,2} = \frac{1}{4} \sum_{a=1}^m (\sigma_{a1}^z + \sigma_{a2}^z)^2. \quad (1b)$$

The gate-based implementation of the QAOA for our problem Hamiltonians in Eqs. (1) can be found in Appendix E. With the above encoding, an instance is satisfied only if the ground state energy is zero. As QAOA minimizes the cost function, it can be considered as an approximate algorithm for solving Max-1- $k$ -SAT<sup>+</sup>. By default, via a threshold decision, the solution of the optimization also implies the solution to the decision version.

Our overall goal in this paper is to understand what is hard and what is easy on QAOA, both in terms of trainability and accuracy.

## III. GRADIENT OF QAOA TRAINING

As a variational circuit, QAOA’s cost-function gradients over variables  $\vec{\gamma}, \vec{\beta}$  indicate the shape of cost-function landscape—larger amplitudes of gradients indicate sharper changes and therefore the problem is easier to train; while small amplitudes of gradients leads to barren plateaus [16, 27–30] that make the training difficult. As gradients average to zero on random states [27, 28], we evaluate the standard deviation (SD) of gradients to characterize their typical amplitudes.

To represent the typical case of training, we evaluate the gradient on random choices of the circuit parameters via a numerical finite-difference. Without loss of generality, we consider the gradient over the first variable  $\gamma_1$  and denote it as  $\partial_1 \mathcal{C}$  [27, 28]. To enable an easier visualization in Fig. 1(c),(d), we plot the inverse of the gradient SD,  $1/\text{SD}(\partial_1 \mathcal{C}(\vec{\gamma}, \vec{\beta}))$ , so that large values indicate hardness

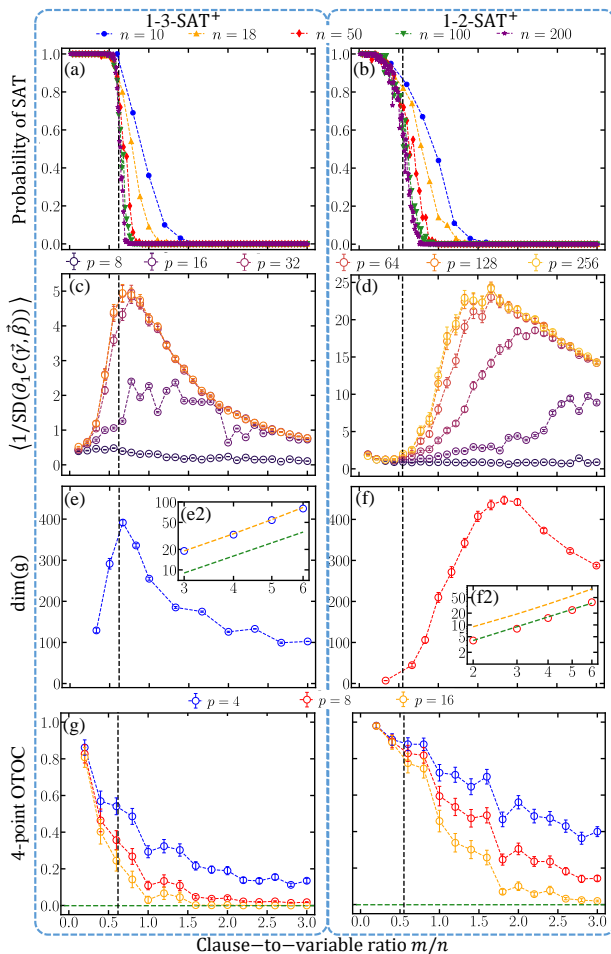


Figure 1. **SAT-UNSAT phase transition and trainability of 1-3-SAT<sup>+</sup> (left column) and 1-2-SAT<sup>+</sup>.** (a)(b) Probability of SAT for different system size  $n$ . (c)(d) The mean of  $1/\text{SD}(\partial_1 \mathcal{C}(\vec{\gamma}, \vec{\beta}))$  in different  $p$ -layer QAOA with  $n = 18$  variables. (e)(f) The dimension of dynamical Lie algebra  $\dim(\mathfrak{g})$  for generators in QAOA in an  $n = 6$  qubits system. The inset log-log plots (e2) and (f2) show  $\dim(\mathfrak{g})$  versus  $n$  with a fully symmetric  $H_C$ . Green and orange curves represent the lower bound estimate  $\dim(\mathfrak{g}) = n^2$  and upper bound of  $\dim^{\text{UB}}$ . (g)(h) Average of 4-point OTOC for different  $p$ -layer QAOA with  $n = 10$  variables. Green horizontal dashed line represents the value given by Haar unitary  $-2^n/(4^n - 1)$ . Vertical dashed lines indicate the critical SAT-UNSAT transition point. All results are evaluated over 100 instances.

in convergence. We consider different number of layers  $p$  in QAOA to obtain a comprehensive picture of it.

For 1-3-SAT<sup>+</sup>, Fig. 1(c) shows a clear peak of inverse gradient SD at around the critical clause-to-variable ratio  $m/n$  indicated by the dashed line, when  $p$  is large. A slight deviation is seen due to the finite size of  $n = 18$ , consistent with the probability transition for the same finite size (orange line) shown in Fig. 1(a). A large inverse gradient SD indicates a small gradient in the typical case, and therefore a more barren plateau that makes the training hard at the phase transition. When  $p$  is small,

the peak disappears; however, at the same time, QAOA fails to provide the accurate solution, making trainability irrelevant.

On the contrary, for 1-2-SAT<sup>+</sup>, Fig. 1(d) shows that the peak of the inverse gradient SD significantly deviates from the critical clause-to-variable ratio  $m/n$  indicated by the dashed line [31]. The deviation is significant even considering the finite-size effect, which indicates that the hard cases, at least in terms of trainability, for QAOA in 1-2-SAT<sup>+</sup> is not those instances at the SAT-UNSAT transition. Such a deviation gives hope to a much better performance of the QAOA in solving 1-2-SAT<sup>+</sup>, as we will show later in the paper.

### A. Connection to controllability

To understand the different behaviors of the gradient, we utilize the connection between gradient and controllability measured by the dimension of dynamical Lie algebra (DLA) of QAOA generators, as recently identified in Ref. [16].

As explained in Ref. [13], DLA can be used to test the controllability of the quantum system governed by unitary dynamics. Let us consider an  $n$ -qubit system described by a Hilbert space  $\mathcal{H}$ . Considering an optimal quantum control model described by a unitary  $U = \prod_{k=1}^K e^{-iu_k H_k}$ , where  $\mathcal{G} \equiv \{H_1, \dots, H_K\}$  is a set of generators and  $\{u_1, \dots, u_K\} \subseteq \mathbb{R}$  is a set of coefficients which are usually represented by the control fields. Then, the DLA  $\mathfrak{g} \equiv \langle iH_1, \dots, iH_K \rangle_{\text{Lie}} \subseteq \mathfrak{su}(2^n)$ , is constructed by the repeated and nested commutators of the elements in  $\mathcal{G}$ . The corresponding dynamical Lie group is therefore obtained by taking the exponential of the DLA  $e^{\mathfrak{g}} \equiv \{e^{V_1} e^{V_2} \dots e^{V_L}, V_1, \dots, V_L \in \mathfrak{g}\}$ . Generally, for a finite-time evolution governed by Schrödinger's equation, the system is fully controllable when the set of the unitaries obtained during this evolution can cover all unitaries as its elements. This is precisely formulated by the so-called Lie algebra rank condition, which states that the system is fully controllable if and only if  $\dim(\mathfrak{g}) = 4^n - 1$  [32]. For quantum systems where the whole Hilbert space is not fully controllable, when the DLA  $\mathfrak{g}$  can be described as the direct sum, i.e.  $\mathfrak{g} = \bigoplus_j \mathfrak{g}_j$ , so that the Hilbert space can be written in a form of the direct sum of the subspace  $\mathcal{H}_j$  as  $\mathcal{H} = \bigoplus_j \mathcal{H}_j$ ,  $\dim(\mathfrak{g}_j)$  determines the subspace controllability of  $\mathcal{H}_j$  [14–16].

With a problem Hamiltonian  $H_C$  and the mixing Hamiltonian  $H_B$  as the generators, we can generate the DLA  $\mathfrak{g}$  and provide an estimate of the standard deviation of gradient from the dimension of the DLA  $\dim(\mathfrak{g})$  as

$$1/\text{SD}(\partial_1 \mathcal{C}(\vec{\gamma}, \vec{\beta})) \in \Omega\left([\text{poly}(\dim(\mathfrak{g}))]^{1/2}\right) \quad (2)$$

where “poly” denotes a polynomial function. Here, for two functions  $f(x)$  and  $g(x)$ ,  $f(x) \in \Omega(g(x))$  means  $f(x)$  is bounded below by  $g(x)$  asymptotically.

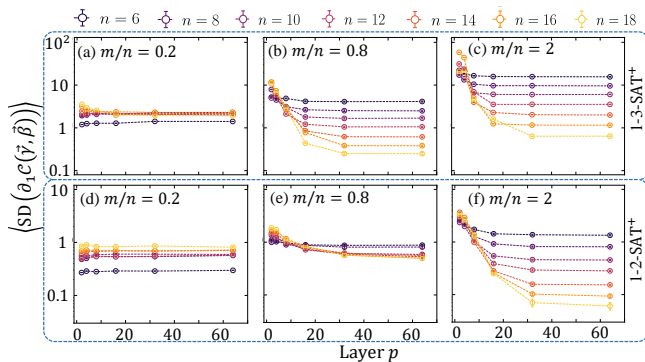


Figure 2. **Barren plateau.** SD of gradient  $\text{SD}(\partial_1 \mathcal{C}(\gamma, \beta))$  versus the layer of QAOA  $p$  for 1-3-SAT<sup>+</sup> (top) for 1-2-SAT<sup>+</sup> (bottom) problems with different number of variables  $n$ . From left to right we plot at three different ratios  $m/n = 0.2, 0.8, 2$ . Due to the finite size  $n \leq 18$ , as shown in Fig. 1 the transition happens at around  $m/n = 0.8$ .

Therefore, we evaluate the DLA dimension numerically to compare with our gradient results. As the numerical evaluation is costly, we are limited to a smaller size of  $n = 6$ . Despite the small size, as we see in Fig. 1 (e) and (f), the DLA dimension  $\dim(\mathbf{g})$  essentially has the same behavior versus the clause-to-variable ratio  $m/n$ , when compared with the inverse gradient; while for 1-3-SAT<sup>+</sup>, the dimension achieves the maximum at the SAT-UNSAT phase transition indicated by the black dashed line, for 1-2-SAT<sup>+</sup> the maximum is achieved well above the SAT-UNSAT phase transition. This manifests a clear connection between the gradient transition and the DLA dimension transition.

An additional insight can be obtained by considering evaluating the DLA dimension at the  $m \gg n$  limit, where the Hamiltonian is symmetric between all qubits (see inset of Fig. 1 (e) and (f)). In this case, we are able to prove an upper bound (see Appendix B),  $\dim(\mathbf{g}) \leq \dim^{\text{UB}} \equiv \frac{1}{6}n(n^2 + 6n + 11)$ . We also expect  $\dim(\mathbf{g})$  to be above  $n^2$ , which is the dimension for a much simpler nearest neighbour Ising model [16]. While the upper bound is in general a loose one, it indicates that the gradient in the  $m \gg n$  limit is only polynomially small; in contrast, for the hard instances we would expect an exponentially small gradient. This contrast supports the decay of dimension and the increase of gradient when  $m/n$  is large.

## B. Barren plateau and complexity

To further understand the barren plateau, in Fig. 2 we plot the SD of gradient versus the layer  $p$  for different number of qubits  $n$ , while keeping the clause-to-variable ratio  $m/n$  to be a constant in each panel. For 1-3-SAT<sup>+</sup>, when  $m/n$  is small in panel (a), the SD of gradient saturates and does not decrease versus  $p$  or  $n$ , showing no barren plateau; At the critical value in panel (b), we see an exponential decrease of SD versus the number of

qubits  $n$  at large  $p$ , confirming a barren plateau. Above threshold, as shown in panel (c), a barren plateau can still be confirmed, however, with larger gradients than the critical case of panel (b). On the contrary, for 1-2-SAT<sup>+</sup> as we see in panel (d) and (e), at around the SAT-UNSAT transition we do not see the appearance of a barren plateau. At large  $m/n$  in panel (f), the gradient finally starts to show an exponential decay, indicating a barren plateau.

The appearance of barren plateaus are often connected to the complexity of the typical quantum circuit involved [28]. The complexity of an ensemble of unitaries can in general be characterized by the closeness to unitary  $t$ -design, which reproduces the Haar random expectation values of  $2t$ -point correlators. In this regard, when the quantum circuit forms a 2-design [17, 18, 33], it has been shown that the variance of the gradient will vanish exponentially with the system size—which leads to a barren plateau of cost function [27, 28].

Therefore, we consider the unitary ensemble  $\mathcal{U}_p$  formed by the  $p$ -layer QAOA,  $U_{\text{QAOA}} = \prod_{\ell=1}^p e^{-i\beta_\ell H_B} e^{-i\gamma_\ell H_C}$ , with each angle  $\gamma_\ell \in [0, 2\pi)$  and each angle  $\beta_\ell \in [0, \pi)$  independent and uniform random. To measure the closeness to 2-design, we evaluate the ensemble-averaged infinite-temperature 4-point out-of-time-order correlator (OTOC)

$$C_{\text{OTOC}}(W_1, W_2; \mathcal{E}) = \frac{1}{d} \langle \text{Tr}\{W_1 U^\dagger W_2 U W_1 U^\dagger W_2 U\} \rangle_{\mathcal{E}}, \quad (3)$$

where the dimension  $d = 2^n$  for an  $n$ -qubit system and the average is over the unitary  $U \in \mathcal{E}$  [18]. For ensemble  $\mathcal{E}$  forming a 2-design, we have  $C_{\text{OTOC}}(W_1, W_2; \mathcal{E}) = -d/(d^2 - 1)$  saturate to the Haar results [18, 33]; while for trivial ensembles,  $C_{\text{OTOC}}(W_1, W_2; \mathcal{E})$  is of order one. Therefore, the decay of OTOC indicates the ensemble being a 2-design. Without loss of generality, we consider the OTOC between single-qubit operators  $C_{\text{OTOC}}(\sigma_1^y, \sigma_{n/2}^y; \mathcal{U}_p)$ . In Fig. 1 (g), we find the OTOC of the QAOA ensemble for 1-3-SAT<sup>+</sup> to decay towards the Haar value when clause-to-variable ratio  $m/n$  increases to the critical value of SAT-UNSAT transition, indicating a transition to 2-design. While similar transition happens well above the SAT-UNSAT transition for 1-2-SAT<sup>+</sup>, as shown in Fig. 1 (h).

## IV. ACCURACY OF QAOA

In this section, we explore the accuracy of QAOA in solving 1- $k$ -SAT<sup>+</sup>. To speedup the training, we develop a heuristic pre-optimization initialization strategy (see Appendix G). To obtain the best accuracy, we perform 10 repetitions on QAOA for each instance to obtain the optimal solution among those results. To benchmark the accuracy of QAOA with the classical algorithm, we reduce the problem to the maximum weighted independent set (MWIS) problem [34, 35] and utilize the greedy ap-

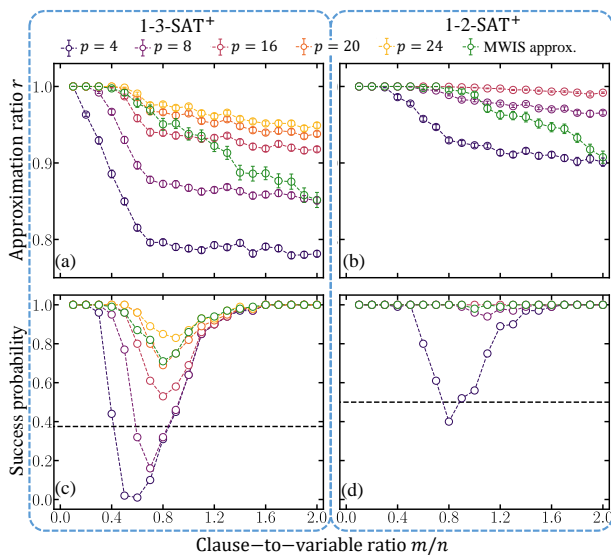


Figure 3. **Accuracy of QAOA.** (a)(b) Approximation ratio  $r$  of SAT clauses, (c)(d) Success probability in determining SAT/UNSAT for 1-3-SAT<sup>+</sup> (left) (from  $p = 4$  to  $p = 24$ ) and 1-2-SAT<sup>+</sup> (right) (from  $p = 4$  to  $p = 16$ ) versus clause-to-variable ratio  $m/n$  with  $n = 10$  variables. Green dots represent the classical approximate results through a reduction to MWIS. The horizontal black dashed line in (c)(d) represent the success probability of the random guess which are  $3/8$  and  $1/2$  for 1-3-SAT<sup>+</sup> and 1-2-SAT<sup>+</sup> separately.

proximate MWIS algorithms proposed in [36, 37] (see Appendix C).

The standard accuracy characterization of approximate algorithms for optimization problem is the approximation ratio [11, 36, 37]. For our case of Max-1- $k$ -SAT<sup>+</sup>, we define the approximation ratio  $r \leq 1$  of a solution to be the ratio between the number of clauses satisfied by the solution and the maximum number of clauses that can be satisfied by any solution. As the output state  $|\psi(\vec{\gamma}, \vec{\beta})\rangle$  in QAOA can be in a superposition of multiple solutions, we evaluate the expected approximation ratio via projecting the output state to the computational basis. A random assignment will satisfy on average  $mk/2^k$  number of clauses, for the instances with most clauses satisfiable, this corresponds to an approximation ratio of  $r_{\text{rand}} \sim k/2^k$ . An exact optimal solution will saturate  $r = 1$  and non-trivial approximate algorithms should have  $r \in [r_{\text{rand}}, 1]$ .

In Fig. 3 (a) and (b), we see that as  $p$  increases, QAOA is able to obtain larger approximation ratios. As the clause-to-variable ratio  $m/n$  increases, the approximation ratio decays as expected. However, the decay is rather slow and manifest a robustness of QAOA. Although both Max 1- $k$ -SAT<sup>+</sup> with  $k = 3$  and  $k = 2$  are NP-hard, the accuracy of QAOA is higher for  $k = 2$  than  $k = 3$  with the same number of  $p$  layers due to the relative lower complexity of  $H_{C,2}$  (see Appendix E).

We also plot the approximation ratio of the classical MWIS approximate algorithm in Fig. 3 for comparison

(see Appendix C). For Max-1-3-SAT<sup>+</sup>, we identify a clear quantum advantage at around  $p \sim 16$ . For Max-1-2-SAT<sup>+</sup>, advantages appear even for a shallow depth of  $p = 8$ . We want to emphasize that the quantum advantage happens only when the clause-to-variable ratio is large, despite the reachability deficits [12]. Indeed, we expect quantum algorithms to be advantageous especially for hard problems, where both classical and quantum algorithms face challenges.

To connect to the empirical hardness transition in classical algorithms, we can also reinterpret each optimization result as a decision of SAT/UNSAT. This can be done via a threshold decision on the minimized number of UNSAT clauses, *e.g.*, determine an instance as SAT when the expected number of UNSAT clauses is smaller than  $E_{\text{th}} = 0.5$  and UNSAT otherwise. To characterize the overall performance, we evaluate the success probability of deciding SAT/UNSAT when solving random instances at a fixed clause-to-variable ratio  $m/n$ . The results are shown in Fig. 3(c) and (d) for  $k = 3$  and  $k = 2$ .

The success probability increases with the layer of QAOA  $p$  as we expect. For 1-3-SAT<sup>+</sup>, there is a valley of low success probability at around the critical point of  $m/n$  shown in Fig. 1(a), recovering the same hardness transition identified in empirical studies of classical algorithms [6–10]. While for the 1-2-SAT<sup>+</sup>, despite a similar valley of low success probability at small  $p$ , the success probability is almost unity for a circuit depth of  $p = 16$ . Similarly, the classical benchmark can be reinterpreted and similar transition versus  $m/n$  can be seen.

Combining the above, we see that overall QAOA possesses a similar notion of what is hard and easy as classical algorithms, while showing advantage over classical algorithms in the large problem-density instances.

## V. GENERALIZATION TO QUANTUM ADIABATIC ALGORITHM

As the quantum computational phase transition for QAOA mimics the classical computational phase transition for classical optimization algorithms, the overall trend reveals the general empirical hardness of SAT instances with different clause-to-variable ratios. Therefore, we expect the same transition to hold in other quantum algorithms. Below we confirm such in QAA—a popular alternative and also the predecessor of QAOA.

To obtain the solution, QAA prepares the ground state of the problem Hamiltonian in Eq. (1) via an adiabatic evolution of the Hamiltonian

$$H(s) = sH_C + (1-s)H'_B, s \in [0, 1], \quad (4)$$

from an ancillary Hamiltonian  $H'_B$  at  $s = 0$  to the problem Hamiltonian  $H_C$  at  $s = 1$ . Here the ancillary Hamiltonian  $H'_B = \sum_{i=1}^n |h_i| \sigma_i^x$ , where  $|h_i|$  is the number of times the variable  $v_i$  appear in the clauses (see Appendix A). The initial Hamiltonian at  $H(0) = H'_B$ , with a easy to prepare ground state  $|\psi(0)\rangle \propto (|0\rangle - |1\rangle)^{\otimes n}$  in

a superposition of all possible spin configurations. As one tunes the parameter  $s$  slowly towards  $H(1) = H_C$ , the adiabatic theorem guarantees that the state of the system stays in the ground state, and therefore the final state  $|\phi_{\text{QAA}}\rangle$  is the ground state of the problem Hamiltonian, which provides the solution to the optimization problem.

From the adiabatic theorem, we can obtain an estimation on the computation time of QAA as  $T_a \sim 1/(\Delta E)^2$  so that the success probability is close to unity, where  $\Delta E$  is the minimum gap of the Hamiltonians  $\{H(s), s \in [0, 1]\}$  [21, 23]. In Fig. 4(a)(b), we evaluate the inverse gap square  $1/(\Delta E)^2$  as a measure of the instance hardness of 1- $k$ -SAT<sup>+</sup> with different clause-to-variable ratio using Qutip [38]. In subplot (a), we identify a similar computational phase transition for 1-3-SAT<sup>+</sup> as QAOA in Fig. 1, where the minimum gap is minimum at about the critical SAT/UNSAT transition, up to some small deviation due to finite size. While for 1-2-SAT<sup>+</sup>, we see the minimum gap to be higher than the critical point, qualitatively agreeing with the case of QAOA in Fig. 1.

To further confirm the transition, we evaluate the success probability  $P = \sum_{i=1}^D |\langle \psi_i | \phi_{\text{QAA}} \rangle|^2$  from the overlap between the final evolved state  $|\phi_{\text{QAA}}\rangle$  and the  $D$ -degenerate ground state of the problem Hamiltonian  $|\psi_i\rangle$ . In Fig. 4(c)(d), at a finite time  $T_a$ , we see the success probability of QAA decreases before the critical point, while roughly maintaining a constant above the critical point. Such a robustness to the problem density coincides with the slow decay of QAOA's approximation ratio with the problem density. In addition, we also find the success probability of 1-2-SAT<sup>+</sup> (subplot (d)) to be much higher than that of 1-3-SAT<sup>+</sup> (subplot (c)).

## VI. DISCUSSION

In this paper, we numerically unveil a computational phase transition in Hamiltonian-based algorithms such as QAOA and QAA when solving SAT problems. Such a phase transition is connected to the controllability and complexity of QAOA circuits. Although our results are empirical, we expect analytical results to be challenging, as the classical correspondence of such transition is also empirical due to the complexity of the SAT problems. We also identify quantum advantages of QAOA against classical greedy approximate algorithms for a relatively small-scale quantum system, potentially realizable in the near-term. Although we have focused on 1- $k$ -SAT<sup>+</sup> for convenience, we expect the computational phase transition in QAOA to apply to all combinatorial optimization problems. In particular, as 1-3-SAT<sup>+</sup> is NP-complete, the clause-to-variable ratio represents a universal characterization of a 'problem density' [12], and the computational phase transition applies to all NP-complete problems in this regard.

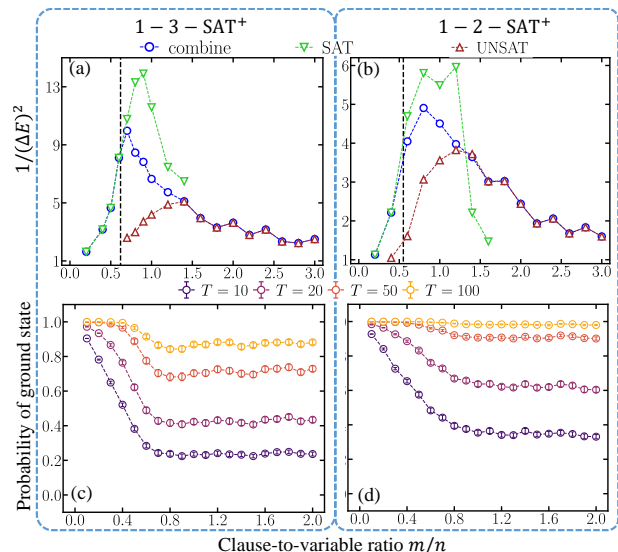


Figure 4. **Gap size and performance of QAA.** (a)(b) The median of  $1/\Delta E^2$  of QAA with  $n = 10$  variables shown by blue circles. The green and purple circles represent the SAT and UNSAT instances separately. (c)(d) The probability that the state through QAA evolution lies in ground state  $P = \sum_{i=1}^D |\langle \psi_i | \phi_{\text{QAA}} \rangle|^2$ .

## ACKNOWLEDGMENTS

This work is supported by Defense Advanced Research Projects Agency (DARPA) under Young Faculty Award (YFA) Grant No. N660012014029, U.S. Department of Energy, Office of Science, National Quantum Information Science Research Centers, Superconducting Quantum Materials and Systems Center (SQMS) under the contract No. DE-AC02-07CH11359, and National Science Foundation (NSF) Engineering Research Center for Quantum Networks Grant No. 1941583. A.S. is supported by the internal R&D from Aliro Technologies, Inc. Q.Z. and A.S. acknowledge helpful discussions with Marco Cerezo and Francesca Albertini.

### Appendix A: Ising formulation of the problem Hamiltonian

Here we introduce the Ising formulation of the problem Hamiltonian in Eqs. (1). For convenience, we first introduce an  $n \times m$  binary matrix  $A_{ij}$ , where  $A_{ij} = 1$  if the variable  $v_i$  is included in the clause  $c_j$  and  $A_{ij} = 0$  otherwise; With this matrix in hand, we can express both Hamiltonians in a two-body Ising form [35] as

$$H_{C,3} = \frac{1}{2} \sum_{i=1}^n h_i \sigma_i^z + \frac{1}{2} \sum_{i<j} J_{ij} \sigma_i^z \sigma_j^z + m, \quad (\text{A1a})$$

$$H_{C,2} = \frac{1}{2} \sum_{i<j} J_{ij} \sigma_i^z \sigma_j^z + \frac{m}{2}, \quad (\text{A1b})$$

where  $h_i = -\sum_{j=1}^m A_{ij}$  and  $J_{ij} = \sum_{a=1}^m A_{ia}A_{ja}$ . The number of clauses containing  $v_i$  is equal to  $|h_i|$ .

## Appendix B: Dynamical Lie algebra: definition and bounds

Below we give bounds for  $\dim(\mathfrak{g})$  in the  $m \gg n$  limit for both 1-2-SAT<sup>+</sup> and 1-3-SAT<sup>+</sup>, where all coefficients  $J_{ij}$ 's and  $h_i$ 's approach uniform (see Appendix D).

For 1-2-SAT<sup>+</sup>, we have  $H_{C,2} \propto \sum_{i<j} \sigma_i^z \sigma_j^z$  up to a constant. Then, the set of the initial generators for the corresponding DLA  $\mathfrak{g}_{H_{C,2},H_B}$  is  $\mathcal{G}_2 \equiv \left\{ \sum_{i=1}^n \sigma_i^x, \sum_{i<j} \sigma_i^z \sigma_j^z \right\}$ . For the fully coupled Ising model with transverse fields along  $x$  and  $y$  axis, the set of the initial generators becomes  $\mathcal{G}_{x,y} \equiv \left\{ \mathcal{G}_2, \sum_{i=1}^n \sigma_i^y \right\}$ . From Ref. [39], the dimension of the corresponding DLA  $\mathfrak{g}_{x,y}$  is

$$\dim(\mathfrak{g}_{x,y}) = \binom{n+3}{n} - 1 = \frac{1}{6}n(n^2 + 6n + 11), \quad (\text{B1})$$

where  $\binom{a}{b} \equiv a!/(a-b)!b!$  is the binomial coefficient. Since the DLAs are generated by the repeated and nested commutators of the generator sets, we must have  $\dim(\mathfrak{g}_{H_{C,2},H_B}) \leq \dim(\mathfrak{g}_{x,y})$  due to  $\mathcal{G}_2 \subset \mathcal{G}_{x,y}$ , which leads to

$$\dim(\mathfrak{g}_{H_{C,2},H_B}) \leq \frac{1}{6}n(n^2 + 6n + 11). \quad (\text{B2})$$

Also we know nearest neighbour Ising model has dimension  $n^2$  [16]. Therefore, we expect the scaling to be between  $\Omega(n^2)$  and  $O(n^3)$ .

For the 1-3-SAT<sup>+</sup>, we have  $H_{C,3} \propto \frac{2}{n-1} \sum_{i<j} \sigma_i^z \sigma_j^z - \sum_{i=1}^n \sigma_i^z$ . Then, the initial set of generators is  $\mathcal{G}_3 = \left\{ \sum_{i=1}^n \sigma_i^x, \frac{2}{n-1} \sum_{i<j} \sigma_i^z \sigma_j^z - \sum_{i=1}^n \sigma_i^z \right\}$ . Let  $\mathfrak{g}_{H_{C,3},H_B}$  be the corresponding DLA. Here, because we can write

$$e^{iH_{C,3}} = e^{i \frac{2}{n-1} \sum_{i<j} \sigma_i^z \sigma_j^z} e^{-i \sum_{i=1}^n \sigma_i^z}, \quad (\text{B3})$$

if we start from the initial set of generator  $\mathcal{G}'_3 = \left\{ \sum_{i=1}^n \sigma_i^x, \sum_{i=1}^n \sigma_i^z, \sum_{i<j} \sigma_i^z \sigma_j^z \right\}$ , we have the corresponding DLA to strictly contain  $\mathfrak{g}_{H_{C,3},H_B}$ . Now, due to the commutator  $[\sum_{i=1}^n \sigma_i^x, \sum_{i=1}^n \sigma_i^y] \propto \sum_{i=1}^n \sigma_i^z$ , the corresponding DLA of  $\mathcal{G}'_3$  becomes exactly  $\mathfrak{g}_{x,y}$ . Therefore, we have  $\dim(\mathfrak{g}_{H_{C,3},H_B}) \leq \dim(\mathfrak{g}_{x,y})$ , which leads to

$$\dim(\mathfrak{g}_{H_{C,3},H_B}) \leq \frac{1}{6}n(n^2 + 6n + 11). \quad (\text{B4})$$

The lower bound estimation  $n^2$  for the dimension of DLA from nearest neighbour Ising model still holds.

## Appendix C: Classical approximate algorithms

To solve Max-1- $k$ -SAT<sup>+</sup>, we transform it to the MWIS problem. Given a 1- $k$ -SAT<sup>+</sup> instance with  $n$  variables

and  $m$  clauses, one can construct a weighted graph with  $n$  vertices  $\{q_i\}_{i=1}^n$ , each corresponding to a variable  $v_i$  and having the weight  $w(q_i) = |h_i| \geq 0$ . For every two distinct vertices  $q_i, q_j$ , an edge  $(q_i, q_j)$  exists if  $J_{ij} > 0$ —when the corresponding variable  $v_i, v_j$  appear in at least one clause at the same time.

One can verify that the SAT/UNSAT version of 1- $k$ -SAT<sup>+</sup> problem is reduced to asking whether the weight of maximum independent set is equal to  $m$  or not. The reason is simple: an independent set of this graph corresponds to an assignment that does not have more than one true assignment in any clause. To guarantee a solution to the 1- $k$ -SAT<sup>+</sup> instance, we still need to make sure that all clauses have one true variable. As the total weight of the independent set is equal to how many clauses are satisfied by this assignment, therefore if the total weight is equal to  $m$ , all clauses are satisfied. At the same time, the Max-1- $k$ -SAT<sup>+</sup> can be reduced to solving the MWIS. As a classical benchmark, we can utilize various greedy algorithms for MWIS [36, 37] and choose the best performance among them (see Appendix F).

## Appendix D: Distribution of Hamiltonian coefficients

In this section, we analytically derive the distribution of coefficients in the problem Hamiltonian  $H_{C,k}$  for both  $k = 3$  and  $k = 2$  (see Eqs. (A1)), and as well as the mean and variance.

For 1-3-SAT<sup>+</sup>, the probability that  $A_{ia}A_{ja} = 1$  for arbitrary two different  $i$  and  $j$  is  $p_3 = (n-2)/\binom{n}{3}$ . According to the definition  $J_{ij} = \sum_{a=1}^m A_{ia}A_{ja}$ , the probability that  $J_{ij} = J$  is

$$P_3(J_{ij} = J) = \binom{m}{J} p_3^J (1 - p_3)^{m-J}, \quad (\text{D1})$$

where we can directly see that the distribution of  $J$  is dependent on the number of variables  $n$  and number of clauses  $m$ . With the distribution of  $J_{ij}$ , the mean and variance are

$$\mathbb{E}_3(J_{ij}) = \frac{6m}{n(n-1)}, \quad (\text{D2a})$$

$$\text{Var}_3(J_{ij}) = \frac{6m(n^2 - n - 6)}{n^2(n-1)^2}. \quad (\text{D2b})$$

Similarly, for 1-2-SAT<sup>+</sup>, the the probability that  $A_{ia}A_{ja} = 1$  for arbitrary two different  $i$  and  $j$  is  $p_2 = 1/\binom{n}{2}$ , and the probability that  $J_{ij} = J$  is

$$P_2(J_{ij} = J) = \binom{m}{J} p_2^J (1 - p_2)^{m-J}, \quad (\text{D3})$$

which is also size-dependent. The mean and variance are

$$\mathbb{E}_2(J_{ij}) = \frac{2m}{n(n-1)}, \quad (\text{D4a})$$

$$\text{Var}_3(J_{ij}) = \frac{2m(n^2 - n - 2)}{n^2(n-1)^2}. \quad (\text{D4b})$$

As the ratio between standard deviation to the mean of  $J_{ij}$  decreases with the clause-to-variable ratio  $m/n$  for fixed  $n$ , we expect in the limit of large  $m/n$ , the coefficients  $J_{ij}$  approach uniform for all  $i, j$ . The same applies to  $h_i$ 's for  $H_{C,3}$ . At the end of the discussion, we want to address the difference between 1- $k$ -SAT<sup>+</sup> and the well-known Sherrington-Kirkpatrick (SK) model in spin glass with the Hamiltonian  $H_{SK} = \sum_{i<j} J_{ij}\sigma_i^z\sigma_j^z$  where  $J_{ij}$  is independently sampled from the standard normal distribution  $\mathcal{N}(0, 1)$  [40].

### Appendix E: Gate-based implementation of QAOA

To implement the Hamiltonian dynamics in QAOA with a quantum circuit, one can decompose the unitary evolution into parallel Pauli-X and Pauli-Z gates as the following

$$\begin{aligned} & \exp\{-i\gamma_k H_{C,3}\} \\ &= \exp\left(-i\frac{\gamma_k}{2} \sum_i h_i \sigma_i^z\right) \exp\left(-i\frac{\gamma_k}{2} \sum_{i<j} J_{ij} \sigma_i^z \sigma_j^z\right) \\ &= \prod_i \exp\left(-i\frac{\gamma_k h_i}{2} \sigma_i^z\right) \prod_{i<j} \exp\left(-i\frac{\gamma_k J_{ij}}{2} \sigma_i^z \sigma_j^z\right). \quad (\text{E1}) \end{aligned}$$

The case of  $H_{C,2}$  is similar, with all  $h_i$ 's equaling zero. The first and second product in Eq. (E1) correspond to parallel Pauli-Z rotation (RZ) and rotation with ZZ interaction (RZZ) gates. Similarly,  $\exp(-i\beta_k H_B)$  is implemented by Pauli-X rotation (RX) gates. We show the implementations in Fig. 5.

For an instance with a given number of variables, more clauses lead to more two-qubit interactions, or equivalently RZZ gates, until saturation to an all-to-all two-body Hamiltonian. A comparison of the number of gates needed in a single layer of problem Hamiltonian evolution versus the clause-to-variable ratio  $m/n$  for both problems can be found in Fig. 6.

Numerically, we implement the QAOA with Qulacs [41], a high-performance quantum computing platform for both Python and C++. We employ the Broyden-Fletcher-Goldfarb-Shanno (BFGS) algorithm [42–45], a gradient-based quasi-Newton method implemented in Scipy [46], to find the optimal parameters  $\vec{\gamma}^*, \vec{\beta}^*$ . Our numerical simulations are performed on the Puma HPC from University of Arizona with 50 cores of AMD Zen2 CPU and 250GB of RAM.

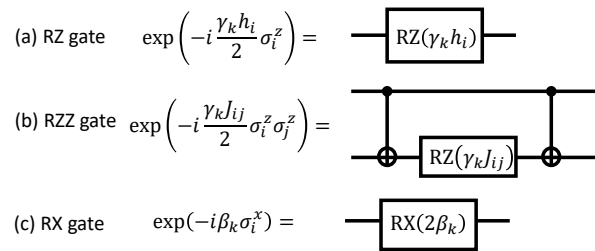


Figure 5. Gate implementations for the evolution under different terms in the Hamiltonians.

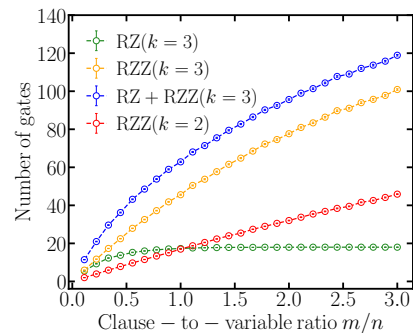


Figure 6. The number of gates in a single layer of problem Hamiltonian evolution in a system of  $n = 18$  qubits for 1- $k$ -SAT<sup>+</sup> with  $k = 3$  and  $k = 2$  versus the clause-to-variable ratio  $m/n$ . Each data point is evaluated over 100 random instances.

### Appendix F: Details of the classical approximate algorithms

Variants of greedy algorithms are proposed for approximate MWIS problems [36, 37]. Before applying those algorithms for benchmark, we introduce some notations to avoid any confusion. Given a weighted graph  $G(Q, E, w)$ , where  $Q, E, w$  represent the set of vertices, edges and weights of vertices, we use  $w(q_i)$  denotes the weight of vertex  $q_i$  and  $w(S)$  denotes the sum of weight for vertex set  $S$ .  $N(q_i)$  represents the set of vertices that are adjacent to vertex  $q_i$  and  $N^+(q_i) = N(q_i) \cup \{q_i\}$ . We denote the degree of vertex  $q$  in graph  $G_i$  as  $d_{G_i}(q)$ .

We briefly summarize the four greedy algorithms that are used for benchmark in this paper, GWMIN, GWMAX, GWMIN2 [36] and WG [37] algorithms. We also list their corresponding guaranteed lower bounds on maximum weight estimation.

#### Algorithm 1 GWMIN

Begin  $S = \emptyset, i = 0, G_i = G$

**while**  $Q(G_i) \neq \emptyset$  **do**

Choose a vertex  $q$  s.t.  $q = \operatorname{argmax}_{u \in Q(G_i)} \frac{w(u)}{d_{G_i}(u)+1}$

$S = S \cup \{q\}$ ; remove  $N_G^+(q)$  from  $G_i$ ;  $i = i + 1$

**end while**

Output  $S$

#### Algorithm 2 GWMAX

Begin  $S = \emptyset, i = 0, G_i = G$   
**while**  $E(G_i) \neq \emptyset$  **do**  
  Choose a vertex  $q$  *s.t.*  
   $q = \operatorname{argmin}_{u \in Q(G_i)} \frac{w(u)}{d_{G_i}(u)(d_{G_i}(u)+1)}$   
  remove  $q$  from  $G_i$ ;  $i = i + 1$   
**end while**  
Output  $S = Q(G_i)$

### Algorithm 3 GWMIN2

Begin  $S = \emptyset, i = 0, G_i = G$   
**while**  $Q(G_i) \neq \emptyset$  **do**  
  Choose a vertex  $q$  *s.t.*  
   $q = \operatorname{argmax}_{u \in Q(G_i)} \frac{w(u)}{\sum_{q \in N_{G_i}^+(u)} w(q)}$   
   $S = S \cup \{q\}$ ; remove  $N_{G_i}^+(q)$  from  $G_i$ ;  $i = i + 1$   
**end while**  
Output  $S$

### Algorithm 4 WG

Begin  $S = \emptyset, i = 0, G_i = G$   
**while**  $Q(G_i) \neq \emptyset$  **do**  
  Choose a vertex  $q$  *s.t.*  
   $q = \operatorname{argmin}_{u \in Q(G_i)} \frac{\sum_{q \in N_{G_i}^+(u)} w(q)}{w(u)}$   
   $S = S \cup \{q\}$ ; remove  $N_{G_i}^+(q)$  from  $G_i$ ;  $i = i + 1$   
**end while**  
Output  $S$

It is also shown that the lower bounds of approximate ratio for those approximate algorithms are

$$r_{\text{GWMIN}} \geq \sum_{q \in Q(G)} \frac{w(q)}{d_G(q) + 1}, \quad (\text{F1a})$$

$$r_{\text{GWMAX}} \geq \sum_{q \in Q(G)} \frac{w(v)}{d_G(q) + 1}, \quad (\text{F1b})$$

$$r_{\text{GWMIN2}} \geq \sum_{q \in Q(G)} \frac{w(q)^2}{\sum_{u \in N_G^+(q)} w(u)}, \quad (\text{F1c})$$

$$r_{\text{WG}} \geq \frac{W(G)}{\sum_{q \in Q(G)} w(N_G(q))/w(G) + 1}. \quad (\text{F1d})$$

To obtain benchmarks, we reduce the  $1-k\text{-SAT}^+$  instances to MWIS instances with igraph [47] and apply the approximate algorithms introduced above to obtain the approximation ratio results in Fig. 7. As all the four algorithms are variants of greedy algorithms, their performances are similar. The lower bounds of those algorithms in Eq. (F1) are also plotted in Fig. 7(a)(b) as a reference. The final benchmark presented in the main paper are obtained from the best approximation ratio among the four algorithms for every fixed clause-to-variable ratio  $m/n$  separately.

## 1. On approximation ratio

Here we provide a brief summary of known facts of the approximation ratio of problems related to the  $1-k$ -

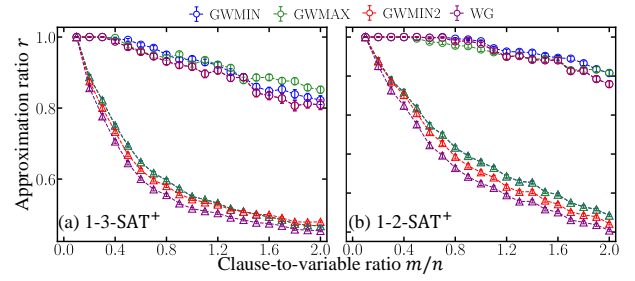


Figure 7. Benchmark on approximate ratio  $r$  with MWIS approximate algorithms for instances reduced from (a)  $1-3\text{-SAT}^+$  and (b)  $1-2\text{-SAT}^+$ . Circles represent approximate ratio  $r$  of different algorithms and triangles represent the corresponding lower bound. All results are fixed with  $n = 10$  variables.

$\text{SAT}^+$ , as there are not much known results for  $1-k\text{-SAT}^+$  itself. Note that these results do not carry over to the  $1-k\text{-SAT}^+$ , as we explain below.

One can reduce a  $1-k\text{-SAT}^+$  instance to a  $k\text{-SAT}$  instance. There is a simple polynomial-time algorithm that provides a  $(1 - 1/2^k)$  approximation ratio for Max- $k\text{-SAT}$  (in this paper we always mean exact  $k$  variables in each clause). This is also equal to the expected approximation ratio of a random assignment. Ref. [11] shows that it is NP-hard to approximate Max-3-SAT above the random assignment threshold of  $7/8 = 0.875$ . Ref. [11] also shows that it is NP-hard to approximate Max-2-SAT with any approximation ratio above  $21/22 \simeq 0.955$ . However, it is important to note that the above are worst case results and does not directly apply to  $1-k\text{-SAT}^+$  due to the reduction.

There are also results on approximate algorithms guaranteeing certain approximate ratios for random instances of Max- $k\text{-SAT}$ . However, as instances generated by reducing the random instances of  $1-k\text{-SAT}^+$  to  $k\text{-SAT}$  are by no means random, these results also do not apply to random instances of Max- $1-k\text{-SAT}^+$ .

## Appendix G: More details on QAOA performance

### 1. QAOA performance and computing time

In the main text, we have provided the approximation ratio results in Fig. 3. Here we also plot the absolute error  $\Delta$  (number of additional violated clauses) in Fig. 8(a) and (b). The optimization steps towards the optimal solution and the computing time are also shown in Fig. 8(c)-(f).

We point out that for  $1-3\text{-SAT}^+$  the ground energy  $E_0$  of  $H_{C,3}$  could be different from the number of violated clauses, because the energy cost of a violated clause can be different among possible spin configurations; While for  $1-2\text{-SAT}^+$  there is no such difference. This difference means that despite  $H_{C,3}$  is a well-accepted Hamiltonian for  $1-3\text{-SAT}^+$  problem [23, 34], there may be other better

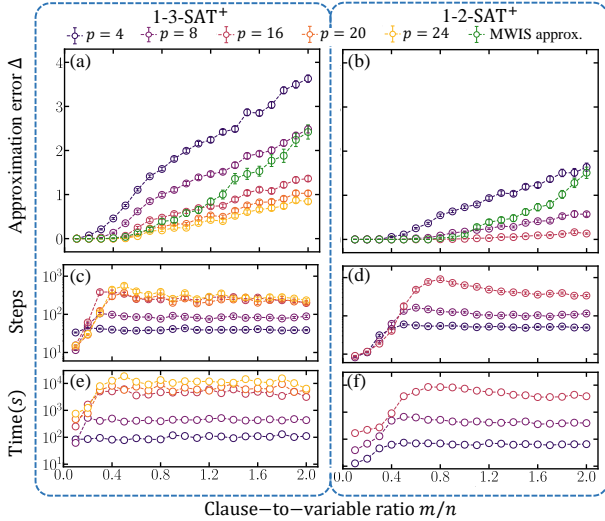


Figure 8. (a)(b) Approximation error  $\Delta$ , (c)(d) optimization steps and (e)(f) CPU time (in seconds) for a  $p$ -layer QAOA versus clause-to-variable ratio  $m/n$  to solve 1-3-SAT<sup>+</sup> (left) and 1-2-SAT<sup>+</sup> (right) with  $n = 10$  variables. Green dots in (a)(b) represent classical approximate solutions obtain by reducing to the MWIS problem.

options.

## 2. Initialization strategy of QAOA

For a  $p$ -layer QAOA, the pre-optimization strategy initializes the first  $p'$  layers ( $1 \leq p' < p$ ) by an optimized  $p'$ -layer QAOA [48], and sample the rest of the parameters  $\{\gamma_k\}_{k=p'+1}^p, \{\beta_k\}_{k=p'+1}^p$  randomly uniformly in  $[0, \epsilon]$ . With the initialization, further training gives the optimal parameters. Here we choose  $\epsilon = 0.1$  to take advantage of the  $p'$ -layer QAOA results without being trapped in local minima.

Now we compare the pre-optimization strategy to a simple random initialization strategy, where all initial parameters  $\{\gamma_k\}_{k=1}^p, \{\beta_k\}_{k=1}^p$  are randomly sampled uniformly in  $[0, \pi]$ . We show the performance on Max-1- $k$ -SAT<sup>+</sup> in Fig. 9(a)(b). Compared to the pre-optimization strategy in Fig. 3(a)(b) of the main paper, the simple random initialization strategy leads to a worse approximation ratio. In particular, as the number of layers  $p$  increases, more parameters need to be optimized and the performance of the random initialization strategy gets much worse than the pre-optimization strategy, especially for  $k = 3$  with a more complex  $H_{C,k}$ . As for the decision version, the performance with the simple random initialization strategy (shown in Fig. 9(c),(d)) is still worse than the performance of the pre-optimization strategy in Fig. 3(c),(d) of the main paper. In Fig. 9(e)-(h), we plot the steps and computing time for the random strategy; Comparing with Fig. 8(c)-(f), we see the computation cost is at the same order of magnitude with the

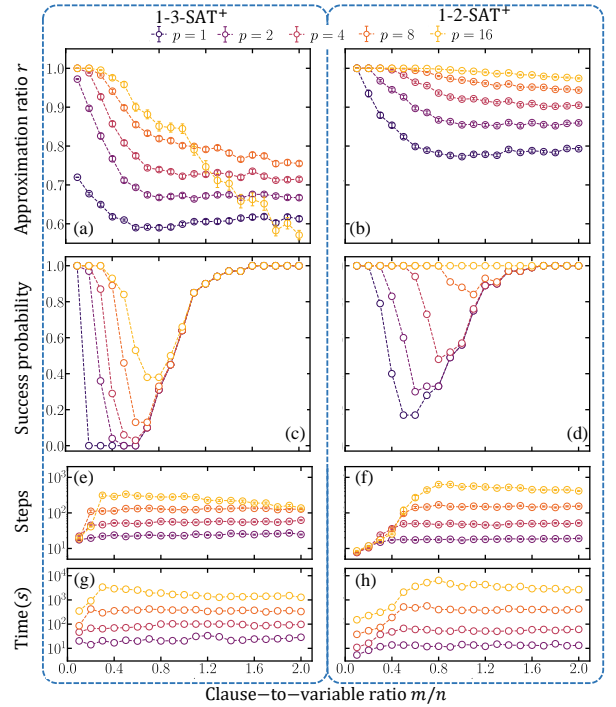


Figure 9. (a)(b) Approximation ratio  $r$ , (c)(d) success probability, (e)(f) optimization steps and (g)(h) CPU computing time (in seconds) for a  $p$ -layer QAOA versus clause-to-variable ratio  $m/n$  to solve 1-3-SAT<sup>+</sup> (left) and 1-2-SAT<sup>+</sup> (right) with  $n = 10$  variables. All results are obtained with the simple random initialization strategy.

pre-optimization strategy.

## 3. Performance with limitations

With the existence of barren plateaus at a large depth, finding the best optimal parameters  $\vec{\gamma}^*, \vec{\beta}^*$  in QAOA consumes a large amount of computing resources for large problem instances. At the same time, the accumulation of errors and noise in near-term devices prohibits a large quantum system to be stable for a long time [2]. Therefore, we consider the sub-optimal performance of QAOA under a cutoff  $T$  on the optimization steps, shown in Fig. 10.

It turns out that for the  $n = 10$  qubit system with  $p = 16$  layers, the performance saturates quickly at only around a hundred steps in most parameter regions. In particular, for the decision version of the problem (Fig. 10 (c)(d)), the easy problems away from the transition only takes a few optimization steps to solve. The only exception is the Max-1- $k$ -SAT<sup>+</sup> problem at large  $m/n$ , where around a thousand steps are necessary. This is due to the optimization versions of the problem being harder at large  $m/n$  ratios, recovering the reachability deficits [12]. Overall, for a given  $p$ , it is efficient to take a limited number of optimization steps in practical implementations to

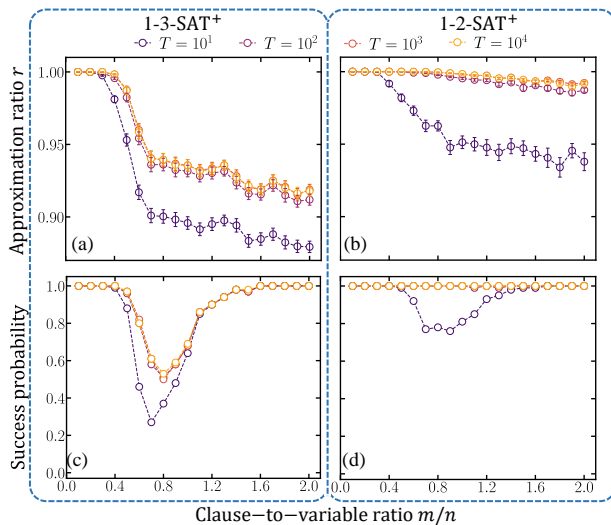


Figure 10. (a)(b) Approximation ratio  $r$  and (c)(d) success probability of a  $p = 16$ -layer QAOA versus clause-to-variable ratio  $m/n$  for 1-3-SAT<sup>+</sup> (left) and 1-2-SAT<sup>+</sup> (right) with  $n = 10$  variables. Dots from dark to light represent the cutoff of optimization steps at  $T = 10, 100, 1000, 10000$ .

get a balance between accuracy and resource consumption.

- 
- [1] E. Farhi, J. Goldstone, and S. Gutmann, A quantum approximate optimization algorithm, arXiv:1411.4028 (2014).
  - [2] J. Preskill, Quantum computing in the nisq era and beyond, *Quantum* **2**, 79 (2018).
  - [3] F. Arute, K. Arya, R. Babbush, D. Bacon, J. C. Bardin, R. Barends, R. Biswas, S. Boixo, F. G. Brandao, D. A. Buell, *et al.*, Quantum supremacy using a programmable superconducting processor, *Nature* **574**, 505 (2019).
  - [4] Y. Wu, W.-S. Bao, S. Cao, F. Chen, M.-C. Chen, X. Chen, T.-H. Chung, H. Deng, Y. Du, D. Fan, *et al.*, Strong quantum computational advantage using a superconducting quantum processor, arXiv:2106.14734 (2021).
  - [5] M. P. Harrigan, K. J. Sung, M. Neeley, K. J. Satzinger, F. Arute, K. Arya, J. Atalaya, J. C. Bardin, R. Barends, S. Boixo, *et al.*, Quantum approximate optimization of non-planar graph problems on a planar superconducting processor, *Nat. Phys.* **17**, 332 (2021).
  - [6] P. C. Cheeseman, B. Kanefsky, W. M. Taylor, *et al.*, Where the really hard problems are., in *IJCAI*, Vol. 91 (1991) pp. 331–337.
  - [7] D. Mitchell, B. Selman, H. Levesque, *et al.*, Hard and easy distributions of sat problems, in *AAAI*, Vol. 92 (Citeseer, 1992) pp. 459–465.
  - [8] D. Achlioptas, A. Chtcherba, G. Istrate, and C. Moore, The phase transition in 1-in-k sat and nae 3-sat, in *Proceedings of the twelfth annual ACM-SIAM symposium on Discrete algorithms* (2001) pp. 721–722.
  - [9] K. Leyton-Brown, H. H. Hoos, F. Hutter, and L. Xu, Understanding the empirical hardness of np-complete problems, *Commun. ACM* **57**, 98 (2014).
  - [10] V. Kalapala and C. Moore, The phase transition in exact cover, arXiv:cs/0508037 (2005).
  - [11] J. Håstad, Some optimal inapproximability results, *J. ACM (JACM)* **48**, 798 (2001).
  - [12] V. Akshay, H. Philathong, M. E. Morales, and J. D. Bi-amonte, Reachability deficits in quantum approximate optimization, *Phys. Rev. Lett.* **124**, 090504 (2020).
  - [13] D. D’Alessandro, *Introduction to Quantum Control and Dynamics*, 1st ed. (Chapman & Hall, 2008).
  - [14] X. Wang, D. Burgarth, and S. Schirmer, Subspace controllability of spin- $\frac{1}{2}$  chains with symmetries, *Phys. Rev. A* **94**, 052319 (2016).
  - [15] D. D’Alessandro, Constructive decomposition of the controllability lie algebra for quantum systems, *IEEE Trans. Automat. Control* **55**, 1416 (2010).
  - [16] M. Larocca, P. Czarnik, K. Sharma, G. Muraleedharan, P. J. Coles, and M. Cerezo, Diagnosing barren plateaus with tools from quantum optimal control, arXiv:2105.14377 (2021).
  - [17] C. Dankert, R. Cleve, J. Emerson, and E. Livine, Exact and approximate unitary 2-designs and their application to fidelity estimation, *Phys. Rev. A* **80**, 012304 (2009).
  - [18] D. A. Roberts and B. Yoshida, Chaos and complexity by design, *J. High Energy Phys.* **2017** (4), 121.
  - [19] A. Nahum, J. Ruhman, S. Vijay, and J. Haah, Quantum entanglement growth under random unitary dynamics, *Phys. Rev. X* **7**, 031016 (2017).
  - [20] Q. Zhuang, T. Schuster, B. Yoshida, and N. Y. Yao, Scrambling and complexity in phase space, *Phys. Rev. A* **99**, 062334 (2019).
  - [21] E. Farhi, J. Goldstone, S. Gutmann, J. Lapan, A. Lundgren, and D. Preda, A quantum adiabatic evolution algorithm applied to random instances of an np-complete problem, *Science* **292**, 472 (2001).
  - [22] A. Young, S. Knysh, and V. Smelyanskiy, First-order phase transition in the quantum adiabatic algorithm,

- Phys. Rev. Lett. **104**, 020502 (2010).
- [23] Q. Zhuang, Increase of degeneracy improves the performance of the quantum adiabatic algorithm, Phys. Rev. A **90**, 052317 (2014).
- [24] D. E. Knuth, Dancing links, arXiv:cs/0011047 (2000).
- [25] M. R. Garey, D. S. Johnson, and L. Stockmeyer, Some simplified np-complete problems, in *Proceedings of the sixth annual ACM symposium on Theory of computing* (1974) pp. 47–63.
- [26] A. Bengtsson, P. Vikstål, C. Warren, M. Svensson, X. Gu, A. F. Kockum, P. Krantz, C. Križan, D. Shiri, I.-M. Svensson, *et al.*, Improved success probability with greater circuit depth for the quantum approximate optimization algorithm, Phys. Rev. Appl. **14**, 034010 (2020).
- [27] J. R. McClean, S. Boixo, V. N. Smelyanskiy, R. Babbush, and H. Neven, Barren plateaus in quantum neural network training landscapes, Nat. Commun. **9**, 4812 (2018).
- [28] M. Cerezo, A. Sone, T. Volkoff, L. Cincio, and P. J. Coles, Cost function dependent barren plateaus in shallow parametrized quantum circuits, Nat. Commun. **12**, 1791 (2021).
- [29] M. Larocca, N. Ju, D. García-Martín, P. J. Coles, and M. Cerezo, Theory of overparametrization in quantum neural networks, arXiv:2109.11676 (2021).
- [30] S. Wang, E. Fontana, M. Cerezo, K. Sharma, A. Sone, L. Cincio, and P. J. Coles, Noise-induced barren plateaus in variational quantum algorithms, Nat. Commun. **12**, 6961 (2021).
- [31] We see the absolute values of the inverse gradient SD have quite different scales in the  $k = 2$  and  $k = 3$  cases. This is because the peaks happen at different  $m/n$  ratios and therefore the absolute values do not match.
- [32] Here, note that we suppose that  $\mathcal{G}$  does not include the identity without the loss of generality because the identity leads to the negligible global phase in QAOA scenario.
- [33] A. Nahum, S. Vijay, and J. Haah, Operator spreading in random unitary circuits, Phys. Rev. X **8**, 021014 (2018).
- [34] V. Choi, Adiabatic quantum algorithms for the np-complete maximum-weight independent set, exact cover and 3sat problems, arXiv:1004.2226 (2010).
- [35] A. Lucas, Ising formulations of many np problems, Front. Phys. **2**, 5 (2014).
- [36] S. Sakai, M. Togasaki, and K. Yamazaki, A note on greedy algorithms for the maximum weighted independent set problem, Discret. Appl. Math. **126**, 313 (2003).
- [37] A. Kako, T. Ono, T. Hirata, and M. M. Halldórsson, Approximation algorithms for the weighted independent set problem, in *International Workshop on Graph-Theoretic Concepts in Computer Science* (Springer, 2005) pp. 341–350.
- [38] J. R. Johansson, P. D. Nation, and F. Nori, Qutip: An open-source python framework for the dynamics of open quantum systems, Comput. Phys. Commun. **183**, 1760 (2012).
- [39] F. Albertini and D. D’Alessandro, Controllability of symmetric spin networks, J. Math. Phys. **59**, 052102 (2008).
- [40] E. Farhi, J. Goldstone, S. Gutmann, and L. Zhou, The quantum approximate optimization algorithm and the sherrington-kirkpatrick model at infinite size, arXiv:1910.08187 (2019).
- [41] Y. Suzuki, Y. Kawase, Y. Masumura, Y. Hiraga, M. Nakadai, J. Chen, K. M. Nakanishi, K. Mitarai, R. Imai, S. Tamiya, *et al.*, Qulacs: a fast and versatile quantum circuit simulator for research purpose, arXiv:2011.13524 (2020).
- [42] C. G. Broyden, The convergence of a class of double-rank minimization algorithms 1. general considerations, IMA J. Appl. Math. **6**, 76 (1970).
- [43] R. Fletcher, A new approach to variable metric algorithms, Comput. J. **13**, 317 (1970).
- [44] D. Goldfarb, A family of variable-metric methods derived by variational means, Math. Comput. **24**, 23 (1970).
- [45] D. F. Shanno, Conditioning of quasi-newton methods for function minimization, Math. Comput. **24**, 647 (1970).
- [46] P. Virtanen, R. Gommers, T. E. Oliphant, M. Haberland, T. Reddy, D. Cournapeau, E. Burovski, P. Peterson, W. Weckesser, J. Bright, *et al.*, Scipy 1.0: fundamental algorithms for scientific computing in python, Nat. Methods **17**, 261 (2020).
- [47] G. Csardi, T. Nepusz, *et al.*, The igraph software package for complex network research, Int. J. complex Syst. **1695**, 1 (2006).
- [48] In practice, the number of layers  $p'$  is chosen to be comparable to  $p$  to obtain better performance.